

Journal Pre-proofs

Scavenging intracellular reactive oxygen species to boost methanol assimilation

Haiyan Liu, Yun Chen, Jian Li, Cheng Zhu, Jiahui Peng, Ramon Gonzalez, Yanfen Bai, Zaigao Tan

PII: S1385-8947(25)04837-5
DOI: <https://doi.org/10.1016/j.cej.2025.164002>
Reference: CEJ 164002

To appear in: *Chemical Engineering Journal*

Received Date: 7 March 2025
Revised Date: 1 May 2025
Accepted Date: 20 May 2025

Please cite this article as: H. Liu, Y. Chen, J. Li, C. Zhu, J. Peng, R. Gonzalez, Y. Bai, Z. Tan, Scavenging intracellular reactive oxygen species to boost methanol assimilation, *Chemical Engineering Journal* (2025), doi: <https://doi.org/10.1016/j.cej.2025.164002>

This is a PDF file of an article that has undergone enhancements after acceptance, such as the addition of a cover page and metadata, and formatting for readability, but it is not yet the definitive version of record. This version will undergo additional copyediting, typesetting and review before it is published in its final form, but we are providing this version to give early visibility of the article. Please note that, during the production process, errors may be discovered which could affect the content, and all legal disclaimers that apply to the journal pertain.

© 2025 Elsevier B.V. All rights are reserved, including those for text and data mining, AI training, and similar technologies.



Scavenging intracellular reactive oxygen species to boost methanol assimilation

Haiyan Liu^{1,2}, Yun Chen^{1,2}, Jian Li^{1,2}, Cheng Zhu^{1,2}, Jiahui Peng^{1,2},
Ramon Gonzalez³, Yanfen Bai⁴*, and Zaigao Tan^{1,2}*

¹ State Key Laboratory of Microbial Metabolism, Shanghai Jiao Tong University, Shanghai, China. 200240.

² Department of Bioengineering, School of Life Sciences and Biotechnology, Shanghai Jiao Tong University, Shanghai, China. 200240.

³ Department of Chemical, Biological and Materials Engineering, University of South Florida, Tampa, FL, USA. 33620.

⁴ Shenzhen Institute of Advanced Technology, Chinese Academy of Sciences, Shenzhen, China. 518000.

Haiyan Liu: yuxihy55@163.com

Yun Chen: chenyun0402ye@163.com

Jian Li: lij0813@163.com

Cheng Zhu: zhuchengshjd@sjtu.edu.cn

Jiahui Peng: 18668900804l@sina.com

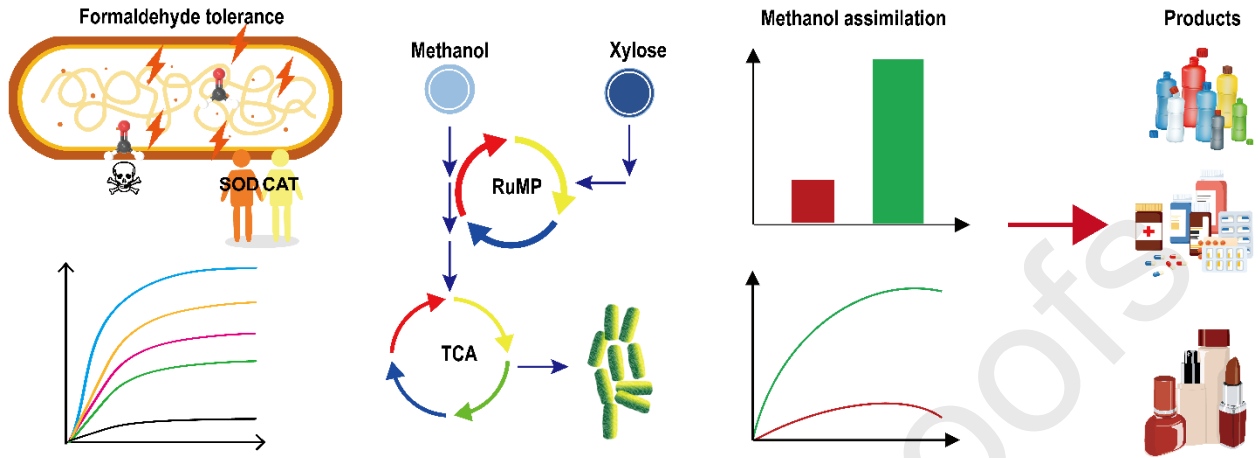
Ramon Gonzalez: ramongonzale@usf.edu

*Corresponding authors: Yanfen Bai: yf.bai@siat.ac.cn; Zaigao Tan, ZTAN0918@sjtu.edu.cn,

Abstract

Formaldehyde, a pivotal yet highly toxic intermediate in most methanol metabolism pathways, has been extensively studied for its cytotoxic effects. Numerous studies have demonstrated that formaldehyde induces significant cellular damage by interfering with fundamental biological processes, including DNA and protein crosslinking. However, the comprehensive understanding of formaldehyde's multifaceted mechanisms of bacterial cell toxicity remains incomplete, which consequently constrains the efficient utilization of methanol. In this study, we identified that formaldehyde accumulation in *Escherichia coli* triggers a substantial elevation in intracellular reactive oxygen species (ROS) levels. Building upon this observation, we systematically investigated the potential advantages of implementing an ROS scavenging system, particularly comprising superoxide dismutase from *Klebsiella pneumoniae* and catalase from *Pseudomonas aeruginosa*, to enhance formaldehyde tolerance. The engineered *E. coli* strain equipped with this ROS detoxification system demonstrated remarkable improvements in both formaldehyde resistance and methanol assimilation efficiency. Notably, the modified strain exhibited a ~30-fold enhancement in methanol assimilation amount (291 mM) compared to the control strain which lacked the ROS scavenging machinery (9 mM) under high amount of methanol. Furthermore, through iterative substrate feeding of methanol and xylose in shake-flask, the engineered strain demonstrated enhanced consumption amount, up to 485 mM (~15.5 g/L). Collectively, our findings underscore the scientific and biotechnological significance of ROS clearance systems in optimizing methanol assimilation, providing valuable insights for metabolic engineering and industrial biotechnology applications.

Graphical abstract



Keywords: Formaldehyde; Reactive oxygen species; Tolerance; Methanol assimilation; High-value products

1. Introduction

The imperative shift toward cleaner energy alternatives, including methanol as a sustainable fuel [1], is driven by the pressing issues of climate change and the ecological drawbacks of fossil fuels [2]. Methanol, recognized for its simplicity as an energy storage molecule [2], serves as an abundant and compatible liquid feedstock for renewable chemical production, seamlessly integrating with existing biomanufacturing and transport systems [3]. Significant advancements have been made in producing methanol from CO₂ via methods, creating value-added chemical process chains with a low or negligible carbon footprint, thereby supporting carbon-neutral objectives [4] (Figure 1A).

The reduction of greenhouse gas (GHG) emissions has heightened interest in methanol as a carbon source for bioprocessing [3]. However, a critical factor in methylotrophic metabolism is the cytotoxicity of methanol intermediates, particularly formaldehyde, serves as a central intermediate in most methylotrophic pathways [5, 6], e.g., RuMP pathway [7], XuMP pathway [8], homoserine cycle [9], MCC pathway [10], FLS pathway [11], SACA pathway [12], HACL pathway [13], ASAP pathway [14], and FORCE pathway [13, 15] (Figure 1A). Formaldehyde is highly toxic, causing chromosomal DNA damage, protein crosslinking and membrane damage [16]. In addition to these detrimental effects, other types of formaldehyde damage to bacterial cells remains unclear.

Reactive oxygen species (ROS), comprising superoxide anion (O₂⁻), hydrogen peroxide (H₂O₂), and hydroxyl radicals (OH⁻), are intrinsic by-products generated during oxygen reduction processes. These highly reactive molecules inflict substantial damage to vital cellular components, including DNA, RNA, proteins, and lipids, culminating in membrane destabilization, protein denaturation, replication impairment, and mutagenesis [17]. Intriguingly, our study has unveiled an additional dimension to the cytotoxic effects of formaldehyde, demonstrating its capacity to induce a pronounced elevation in intracellular ROS levels. Considering this discovery, we sought to mitigate formaldehyde-induced cytotoxicity through the targeted scavenging of intracellular ROS. Remarkably, this intervention not only ameliorated cellular toxicity but also significantly enhanced methanol assimilation efficiency, consequently improving the bioproduction of methanol-derived compounds.

2. Methods

2.1 Strains and plasmids

All plasmids and strains used in this study are listed in Table S1, S2. *Escherichia coli* (*E. coli*) DH5 α was used for plasmid construction and propagation. Strains derived from *E. coli* MG1655 were used for formaldehyde tolerance evaluation, while those derived from *E. coli* MG1655(DE3) were employed for investigating methanol assimilation. The genes *Bm sodA*, *Me sodB*, *Op sod*, *Yl sod2*, *Kp sodB*, *Bm katA*, *Cn katG*, *Mt katG*, *Cb CTAI*, and *Pa katA* were individually integrated into the *pta* locus of the *E. coli* MG1655 genome, which used for formaldehyde tolerance assay. The plasmid pCDF-*mdh-hps-phi*, retrieved from laboratory storage, was employed in methanol assimilation studies. The plasmids PET-*mcrC-mcrN* and pTrc99a-*bktB*, sourced from laboratory storage, were employed for 3-HP and TAL production, respectively.

The CRISPR-Cas9 system[18] was employed for chromosomal editing, enabling the integration of genes *Kp sodB* and *Pa katA*, and the targeted knockout of genes *frmA*, *rpiA*, and *rpiB*. Additionally, the one-step inactivation method (FLP-FRT)[19] was applied to disrupt the *cyaA* gene. The genes *Kp sodB* and *Pa katA* were integrated either individually or in combination into *pta* loci of the *E. coli* MG1655 genome. The expression levels of the *Kp sodB* and *Pa katA* genes were modulated through the use of RBS engineering[20]. Using ‘GTTTAAACCAGGAGRNNNNNN’ as the template sequence[21], a RBS library was constructed, incorporating RBS sequences with varying expression strengths. They were used to optimize the combination of the *Kp sodB* and *Pa katA* genes, which were then integrated into the *pta* loci of the *E. coli* MG1655 genome. As a result, a series of *pta* site integration strains, designated as SC1, SC2, SC3, SC4, SC5, SC6, SC7, and SC8, were constructed. And the strain MG1655 Δ *pta* was obtained from laboratory storage. All the aforementioned strains were subjected to formaldehyde tolerance assays.

A tolerance module of strain SC6, *Kp sodB*-RBS6-*Pa katA*, was integrated into the *pta* locus of the *E. coli* MG1655(DE3) Δ *frmA* Δ *rpiA* Δ *cyaA* genome, resulting in the construction of methanol-assimilating strain AM1. The laboratory-stored strain *E. coli* MG1655(DE3) Δ *frmA* Δ *rpiA* Δ *cyaA* Δ *pta* was designated as AM0. The methanol assimilation performance of these strains was systematically evaluated through experimental analysis.

2.2 Formaldehyde tolerance assay

All tolerance test strains were cultivated in a MOPS-based minimal medium supplemented with 2% (wt/v) glucose, which included 40 mM MOPS, 4 mM tricine, 0.01 mM FeSO₄, 9.5 mM NH₄Cl, 0.276 mM K₂SO₄, 0.5 μ M CaCl₂, 0.525 mM MgCl₂, 50 mM NaCl, 0.292 nM (NH₄)₂MoO₄, 40 nM H₃BO₃, 3.02 nM CoCl₂, 0.962 nM CuSO₄, 8.08 nM MnCl₂, 0.974 nM ZnSO₄, and 1.32 mM K₂HPO₄[22]. The strains were cultured in MOPS minimal medium supplemented with 0 mM or 1 mM formaldehyde, and subjected to continuous kinetic cultivation in microplate reader. Optical density at OD₆₀₀ was monitored, and differences in formaldehyde tolerance were evaluated

based on growth performance. Tolerance testing for high concentrations of formaldehyde (1.2 mM) was conducted in test tubes, with OD₆₀₀ measurements taken.

2.3 Methanol assimilation assay

All strains used in methanol assimilation experiments were cultured in MOPS medium supplemented with 50 mM xylose, 2% (wt/v) casamino acids, and varying concentrations of methanol, and 0.1 mM IPTG to induce the expression of the plasmid pCDF-*mdh-hps-phi*. Additionally, 25 mg/L kanamycin and 50 mg/L spectinomycin were added as required. The strains were cultured in 250 mL baffled shake flasks. During the cultivation process, samples were collected at regular daily intervals for optical density measurements and subsequent analytical assessments.

2.4 Assessment of cellular ROS levels

Cellular ROS was measured using 2,7-dichlorodihydrofluorescein diacetate (DCFH-DA)[23]. The collected bacterial suspension was centrifuged to remove the supernatant and washed twice with PBS buffer to eliminate residual formaldehyde. The cells were then resuspended in PBS buffer, and DCFH-DA dissolved in DMSO was added to achieve a final concentration of 10 µM. The mixture was incubated at 37°C for 1 hour, followed by centrifugation to remove the supernatant. The cells were washed twice with PBS buffer and resuspended in PBS buffer. Fluorescence was measured at an excitation wavelength of 488 nm and an emission wavelength of 525 nm.

2.5 Quantification of Methanol and Xylose Consumption

The consumption of methanol and xylose was detected using an Agilent 1260 HPLC equipped with a refractive index detector (RID). An Agilent Hi-Plex column was employed, with the following chromatographic conditions: 5 mM sulfuric acid as the mobile phase, a refractive index detector temperature of 35°C, a column temperature of 60°C, and a flow rate of 0.6 mL/min.[24]

2.6 C¹³-labeled methanol experiment

The strain AM1 were cultivated in MOPS minimal medium supplemented with 120 mM C¹³-labeled methanol, 50 mM xylose, 2% (w/v) casein hydrolysate, and 0.1 mM IPTG to induce the expression of the plasmid pCDF-*mdh-hps-phi*. Furthermore, 25 mg/L kanamycin and 50 mg/L spectinomycin were added as selective agents where required.

The strain was cultured for six days, after which the cells were harvested through centrifugation. The collected cells were hydrolyzed by treating it with 1 mL of 6N hydrochloric acid at 95 °C for 24 hours. Following hydrolysis, the samples were dried at 95 °C and subsequently re-dissolved in 1 mL of deionized water (ddH₂O). Amino acids released from the hydrolysis were separated using ultra-performance liquid chromatography (UPLC) on a C18 reversed-phase

column (Agilent). Mass spectrometry analysis was performed using an Exactive mass spectrometer (Agilent), and the resulting data were processed with MassHunter software (Agilent)[25, 26].

2.7 Analysis of 3-HP and TAL content

The 3-HP and TAL-producing strains were cultivated in MOPS medium supplemented with 600 mM methanol, 50 mM xylose, and 2% (w/v) casein hydrolysate. Fermentation samples for 3-HP were collected at regular intervals and analyzed using an Agilent 1260 HPLC system, equipped with a DAD detector and an Hi-Plex column. The analytical conditions were as follows: 5 mM sulfuric acid as the mobile phase, UV detection at 210 nm, a flow rate of 0.6 mL/min, and a column temperature maintained at 55°C[27]. The analysis of TAL fermentation samples was conducted according to a previously reported method, involving the collection of the supernatant by centrifugation followed by the measurement of absorbance at 282 nm[28].

3. Results

3.1 Mining and recruiting SOD and CAT enzymes for scavenging intracellular ROS

To initiate our investigation, we conducted comprehensive formaldehyde toxicity assays in *E. coli* to evaluate its cytotoxic effects. Our findings indicated that formaldehyde had pronounced inhibitory effects on *E. coli*, with a concentration as low as 1.25 mM being sufficient to impede growth in MOPS medium supplemented with 2% (wt/v) glucose (Fig. 1B). We are interested in investigating whether formaldehyde causes ROS damage to bacterial cells. Hence the ROS levels in *E. coli* were initially tested in the presence of formaldehyde. The ROS levels in cells increased progressively with the addition of various concentrations of formaldehyde. Specifically, upon adding 1.25 mM formaldehyde, intracellular ROS levels were 2.2-fold higher compared to those in the absence of formaldehyde (Fig 1C), highlighting a significant elevation due to formaldehyde toxicity.

To this end, we sought to scavenge intracellular ROS and thus focused on overexpressing enzymes involved in the ROS scavenging system. The system comprises superoxide dismutase (SOD)[29] and catalase (CAT)[30] (Fig 1D, 1F). Therefore, SOD and CAT from different sources were mined through the databases such as BRENDA and UniProt. Based on the phylogenetic tree analysis, SOD and CAT with distant evolutionary relationships will be selected as candidates for tolerance testing (Fig 1E, 1G). As this study focuses on the efficient conversion of methanol; therefore, the selection of SOD and CAT were preferentially focused on those from methylotrophic organisms. In the SOD screening, SodA from *Bacillus methanolicus* (*Bm soda*) and SodB from *Methylobacterium extorquens* (*Me sodB*) were selected, both of which are methylotrophic bacteria. Additionally, SOD from *Ogataea polymorpha* (*Op sod*) and Sod2 from *Yarrowia lipolytica* (*Yl sod2*) were chosen, as they are methylotrophic yeasts. Furthermore, SodB from *Klebsiella*

pneumoniae (*Kp sodB*), a non-methylotrophic bacterium, was also included as a candidate (Fig 1E). These protein sequences exhibit 42% sequence identity (Fig S1), suggesting that they may display significantly different levels of formaldehyde tolerance.

For the selection of CAT, KatA from *Bacillus methanolicus* (*Bm katA*), KatG from *Cupriavidus necator* (*Cn katG*), and KatG from *Methylosinus trichosporium* (*Mt katG*) were chosen as candidates from methylotrophic bacteria. Additionally, CTA1 from the methylotrophic yeast *Candida boidinii* (*Cb CTA1*) and KatA from the non-methylotrophic bacterium *Pseudomonas aeruginosa* (*Pa katA*) were also selected (Fig 1G). Similarly, due to the very low protein homology, only 23% sequence identity (Fig S2), it is anticipated that they will exhibit distinct formaldehyde tolerance profiles.

Compared to plasmid expression, genome integration offers greater stability and reduces intercellular heterogeneity, eliminating the requirement for antibiotics[31]. Therefore, the 10 SOD or CAT enzymes from different sources were individually integrated into the *pta* locus of the MG1655 genome. The strains were cultivated in MOPS medium supplemented with 2% (v/v) glucose, and continuous kinetic analysis was conducted using a microplate reader. In comparison to the control strain (with *pta* gene knockout), the SodB derived from *K. pneumoniae* (*Kp SodB*) demonstrated a marked advantage in performance. The optical density at 600 nm (OD_{600}) was observed to be 1.5-fold higher in the strain after 14 h of cultivation (0.37), compared to the control strain (0.15) (Fig 1H). The strain carrying KatA from *Pseudomonas aeruginosa* exhibited a growth level ($OD_{600} = 0.72$) 3.9-fold higher than the control strain (Fig 1I). These enzymes catalyze a sequential reaction pathway, where SOD first converts O_2^- into H_2O_2 [32], followed by CAT reducing the H_2O_2 to H_2O [33].

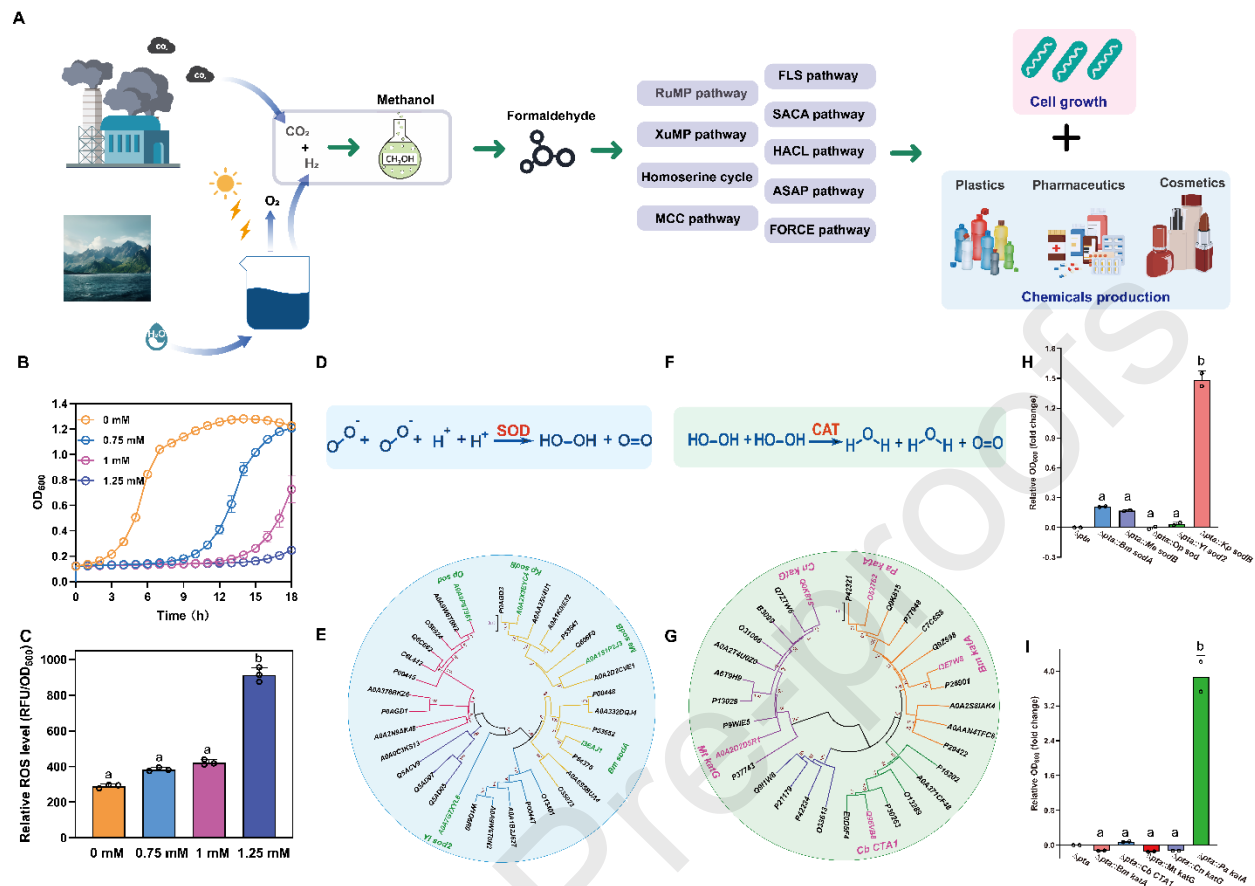


Fig. 1. Screening for formaldehyde tolerance in SDO and CAT from different sources. (A) Schematic flowchart of methanol chemical synthesis and microbial utilization for chemical production. (B) Detection of OD_{600} in *E. coli* MG1655 under different formaldehyde concentrations. (C) Detection of ROS levels in *E. coli* MG1655 under different formaldehyde concentrations. (D) Reaction equation catalyzed by superoxide dismutase (SOD). (E) Phylogenetic tree representing the evolutionary relationships of SOD, verdant labeling demarcates enzymic candidates identified through formaldehyde tolerance screening protocols. (F) Reaction equation catalyzed by catalase (CAT). (G) Phylogenetic tree representing the evolutionary relationships of CAT, fuchsia typography denotes enzymic candidates identified through formaldehyde tolerance screening protocols. (H) Fold changes in OD_{600} of the engineered strains compared to the control strain (*E. coli* MG1655 with the *pta* gene knockout) for SOD. (I) Fold changes in OD_{600} of the engineered strains compared to the control strain (*E. coli* MG1655 with the *pta* gene knockout) for CAT. Different lowercase letters (a, b) indicate significant differences among groups ($p < 0.001$) based on the Games-Howell multiple comparison test.

3.2 Synergistic harnessing SOD and CAT enzymes for further increasing formaldehyde tolerance

Given that SOD and CAT enzymes individually demonstrated effectiveness in mitigating

formaldehyde-induced toxicity, we hypothesized that their synergistic interaction could further enhance cellular tolerance to formaldehyde. To assess this, the *Kp sodB* and *Pa katA* genes were co-expressed. For fine-tune their expression, a series of ribosome binding site (RBS) variants with different strengths were strategically engineered (Fig 2A), enabling precise control over the expression balance between the two enzymes. All the strains displayed similar growth patterns except the strain SC5 under the 0 mM formaldehyde conditions (Fig S3A). As expected, in the presence of 1mM formaldehyde, the engineered strains integrated SOD and CAT at the *pta* site displayed dynamic distinct growth trends and shorter lag times than the control strain (Fig S3B). Specifically noted, at 14 h, the OD₆₀₀ of the strain SC6 reached 0.84, surpassing that of the single-gene expressing strains (*Kp sodB* at 0.37 and *Pa katA* at 0.72) as well as the control strain (0.15) (Fig 2B).

Subsequently, the engineered strain SC6 and the control strain were further evaluated in the test tubes. In the absence of formaldehyde, the engineered strain SC6 exhibited a growth pattern comparable to the control strain. However, under exposure to 1.2 mM formaldehyde, the control strain displayed markedly reduced growth, with an OD₆₀₀ of only 0.2 after 28 h of cultivation. In contrast, the engineered strain SC6 (OD₆₀₀ at 2.4) reached OD values comparable to those obtained in the absence of formaldehyde (Fig 2C, S4). Subsequent analysis assessed ROS levels in those strains. In the absence of formaldehyde, all strains exhibited relatively low ROS levels. However, upon exposure to 10 mM formaldehyde, ROS levels in the control strain increased markedly, and the SC6 strain demonstrated a 52% reduction in ROS accumulation compared to the control strain, despite exhibiting elevated ROS levels (Fig 2D). These results demonstrate that SOD and CAT synergistically improve formaldehyde tolerance.

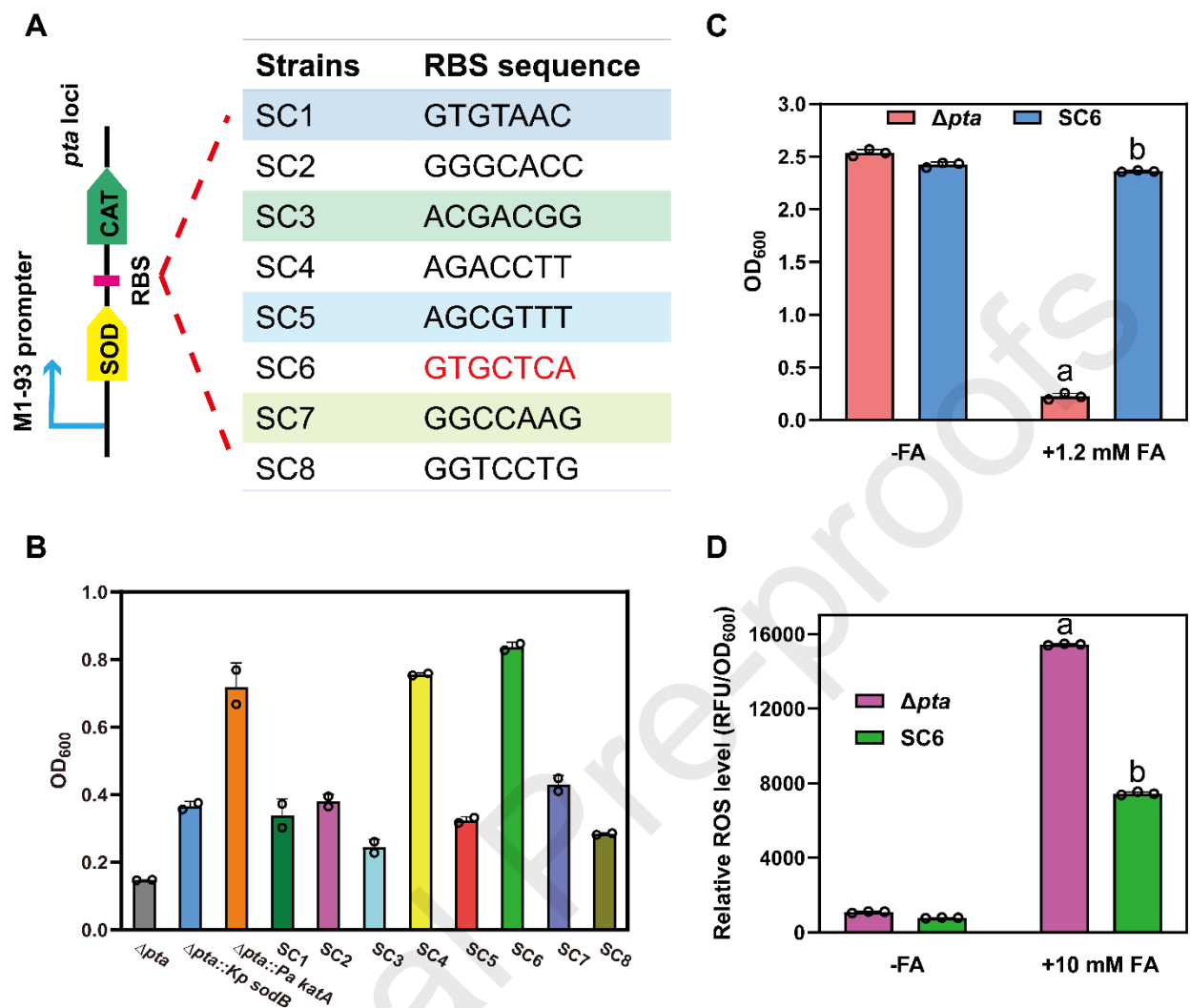


Fig. 2. Assessment of formaldehyde tolerance through the combined expression of SOD and CAT. (A) Left panel: schematic diagram of genetic loci involved in the ROS scavenging system; right panel: screening of the RBS library led to the identification of RBS sequences with varying strengths, with the sequences depicted in the figure corresponding to randomly mutated sites. (B) The strains growth in a microplate reader: 1 mM formaldehyde, for 14 h cultivation. (C) Formaldehyde tolerance characterization in the tubes. (D) ROS level assay under formaldehyde -treated and untreated conditions. Different lowercase letters (a, b) indicate significant differences among groups ($p < 0.001$) based on the Games-Howell multiple comparison test.

3.3 Enhanced ROS-scavenging for augmenting methanol assimilation

Given the remarkable formaldehyde tolerance exhibited by strain SC6, we aimed to leverage this capability to enhance methanol assimilation efficiency. To achieve this, we genetically engineered the strain by integrating a well-characterized methanol assimilation pathway, RuMP

pathway, thereby optimizing its metabolic potential for methanol utilization. This pathway incorporated key enzymes, including methanol dehydrogenase (Mdh), 3-hexulose-6-phosphate synthase (Hps), and 6-phospho-3-hexulose isomerase (Phi) (Fig 3A). In particular, the *mdh* gene from *Cupriavidus necator*[34] and the *hps* and *phi* genes from *Bacillus methanolicus*[35] were integrated into the pCDFduet-1 vector, resulting in the recombinant plasmid pCDF-*mdh-hps-phi* (designated as pCDF-RuMP).

For driving more methanol assimilation, the glutathione-dependent formaldehyde dehydrogenase (*frmA*) gene was selectively disrupted to block the conversion of formaldehyde to formate in the strain SC6, thereby preventing its further oxidative degradation[36]. Given that the RuMP pathway requires D-ribulose 5-phosphate (Ru5P) as a precursor, the availability of this substrate was further optimized by supplementing the strain with xylose. Since wild-type *E. coli* can utilize xylose as the sole carbon source, the strategic deletion of the *rpiAB* genes was employed to inhibit the conversion of Ru5P to ribose 5-phosphate (R5P), thereby channeling the assimilation of xylose exclusively through the RuMP pathway[36]. Moreover, the *cyaA* gene, which encodes adenylate cyclase, was deleted, as it is hypothesized to facilitate methanol utilization through the downregulation of enzymes involved in the TCA cycle[37](Fig 3B). Through a series of genetic manipulations, the strain *E. coli* MG1655(DE3) Δ *frmA* Δ *rpiAB* Δ *cyaA* (referred to as A0) was constructed. The previously established efficient ROS clearance system was then introduced into this strain. As a result, a new strain was generated: *E. coli* MG1655(DE3) Δ *frmA* Δ *rpiAB* Δ *cyaA* Δ *pta::KpsodB-RBS6-Pa katA* (referred to as A1).

To evaluate methanol assimilation, the strains AM1(the strain A1 carrying the plasmid pCDF-RuMP) and AM0 (the strain *E. coli* MG1655(DE3) Δ *frmA* Δ *rpiAB* Δ *cyaA* Δ *pta* carrying the plasmid pCDF-RuMP) were cultivated in MOPS minimum medium supplemented with varying concentrations of methanol, 50 mM xylose, and 2% (wt/v) casein hydrolysate. In shake flasks cultivation, the engineered strain consistently exhibited a vigorous growth profile (Fig S5). After 6 days of cultivation, the OD₆₀₀ of the strain AM1 reached 5.0 in the presence of 300 mM methanol. By comparison, the control strain AM0 exhibited an OD₆₀₀ of only 1.1 (Fig 3C, S6). Due to the volatility of methanol, a blank control group without bacterial inoculation was established. After 6 days of cultivation, methanol in the blank group decreased by 11 mM. The strain AM1 consumed 111 mM, while the control strain AM0 consumed only 29 mM (Fig 3D). For xylose consumption, the strain AM1 retained a small amount of xylose, whereas the control strain consumed only 4 mM (Fig S6).

Interestingly, under 600 mM methanol conditions, the engineered strain exhibited improved growth and more efficient methanol assimilation. After 2 days of cultivation, the strain AM1 reached peak growth, exhibiting OD₆₀₀ values of 8.2—representing increases of 20.8-fold compared to the control strain AM0 (OD₆₀₀ = 0.4) (Fig 3E, S7). With respect to methanol consumption, the strain AM1 demonstrated an even higher methanol consumption of 238 mM, reflecting an 18.8-fold increase compared to the control strain, which utilized only 12 mM of methanol (Fig 3F). The strain AM1 fully consumed the available xylose within 2 days, whereas

the control strain utilized only a negligible amount (Fig S7).

Subsequently, these strains were cultured in a medium containing 900 mM methanol, where the engineered strain AM1 achieved the highest OD_{600} of 6.7 after 3 days of cultivation. However, the control strain exhibited an OD_{600} of only 0.3 (Fig 3G, S8). Throughout the 6-day cultivation, the strain AM1 demonstrated a total methanol consumption of 291 mM, representing a ~30-fold increase relative to the control strain (9 mM) (Fig 3H). During a 3-day cultivation period, the strain AM1 had nearly exhausted all available xylose. In contrast, the control strain showed minimal xylose utilization (Fig S8). These results strongly demonstrate the efficient methanol assimilation capacity of the engineered strain AM1.

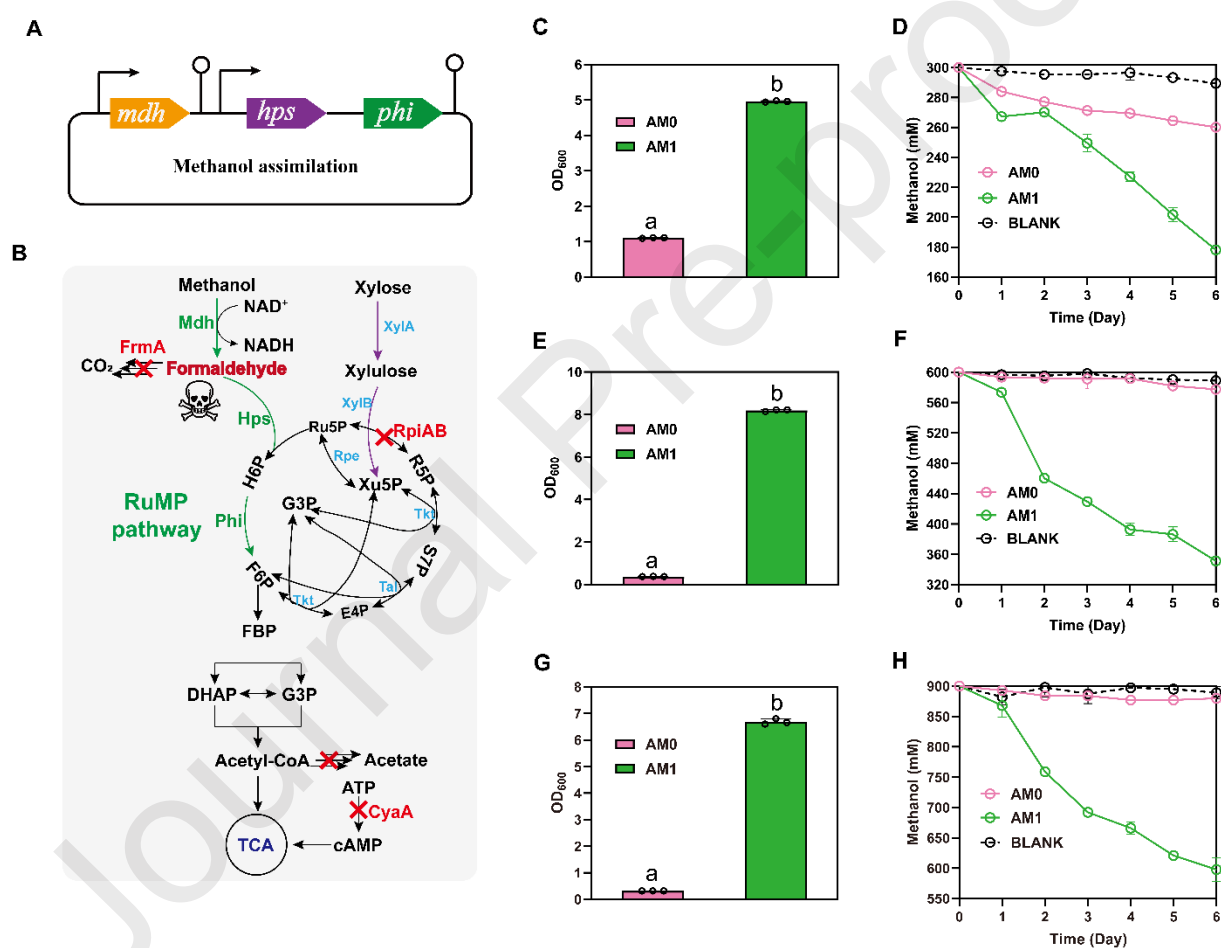


Fig. 3. Enhancing cellular ROS scavenging capacity to improve formaldehyde assimilation. (A) Modular organization of methanol assimilation genes on the expression vector. (B) Schematic diagram of the methanol assimilation-linked central carbon metabolic pathway. Red marking with an X indicates gene knockouts, while green segments represent heterologously introduced RuMP pathway genes, including methanol dehydrogenase (Mdh) from *Cupriavidus necator* and 3-hexulose-6-phosphate synthase (Hps) and 6-phospho-3-hexulose isomerase (Phi) from *Bacillus methanolicus*. Blue segments denote endogenous genes. FrmA, S-(hydroxymethyl) glutathione dehydrogenase; RpiAB, ribose-5-phosphate isomerase A, allose-6-phosphate isomerase; CyaA,

adenylate cyclase; XylA, xylose isomerase; XylB, xylulokinase; Rpe, ribulose-phosphate 3-epimerase; Tkt, transketonase; Tal, transaldolase. (C) 300 mM methanol, the growth of the strains in the baffled shake flasks. (D) 300 mM methanol, the methanol consumption of the strains in the baffled shake flasks. (E) 600 mM methanol, the growth of the strains in the baffled shake flasks. (F) 600 mM methanol, the methanol consumption of the strains in the baffled shake flasks. (G) 900 mM methanol, the growth of the strains in the baffled shake flasks. (H) 900 mM methanol, the methanol consumption of the strains in the baffled shake flasks. Different lowercase letters (a, b) indicate significant differences among groups ($p < 0.001$) based on the Games-Howell multiple comparison test.

At methanol concentrations of 600 mM or 900 mM, the engineered strain rapidly depleted the available xylose. In the subsequent stages, the absence of xylose as a co-carbon source led to a pronounced decline in optical density, accompanied by a substantial decrease in methanol consumption (Fig S7, S8). To further stimulate the methanol assimilation of the engineered strain, additional xylose and methanol were supplemented to the engineered strain AM1. Under conditions of 600 mM methanol, 30 mM xylose was supplemented from 2nd to 9th, with additional 100 mM methanol provided on the 5th and 7th days. This approach resulted in the highest optical density and methanol consumption of the strain AM1, which reached a peak OD₆₀₀ of 12.1 and consumed a total of 485mM methanol and 159 mM xylose over a 9-day cultivation, and the methanol to xylose consumption ratio was 3.8:1(Fig 4A). In the presence of 900 mM methanol, 30 mM xylose was supplemented from 2nd to 5th, followed by 20 mM on 8th, the strain AM1 achieved a maximum optical density of 11.4 and consumed a total of 433 mM methanol and 164 mM xylose over a 9-day cultivation, and the methanol to xylose consumption ratio was 2.6:1(Fig 4B). As far as we are aware, this may represent one of the highest levels of methanol consumption documented among all *E. coli* strains known to assimilate methanol[36-41].

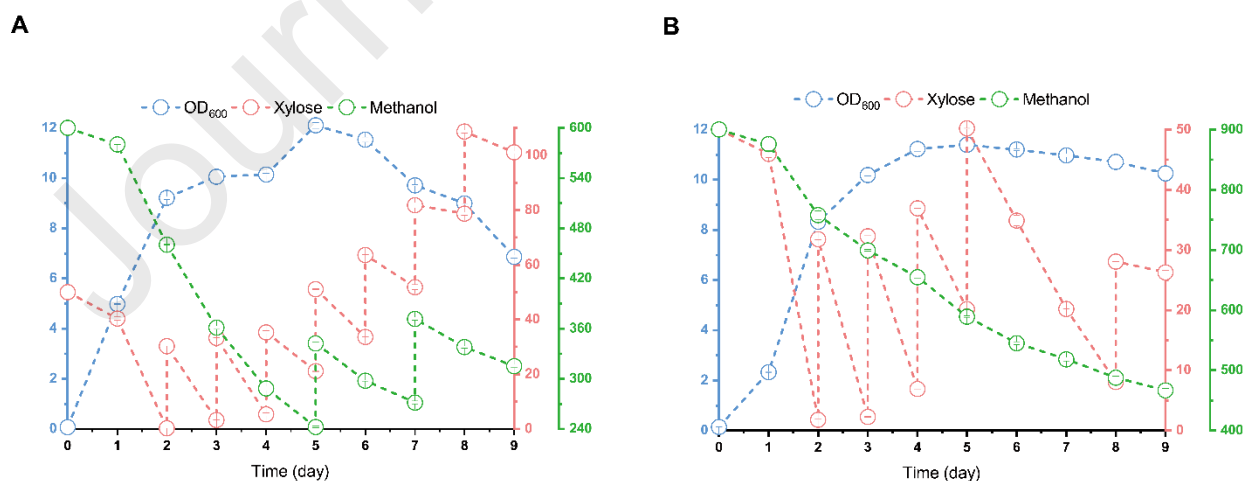


Fig. 4. Fermentation assay with additional xylose supplementation in shake flasks. (A) 600 mM methanol,

the analysis of OD₆₀₀, methanol and xylose consumption in the baffled shake flasks when extra added xylose and methanol for the strain AM1. (B) 900 mM methanol, the analysis of OD₆₀₀, methanol and xylose consumption in the baffled shake flasks when extra added xylose for the strain AM1.

3.4 Metabolic profile in efficient methanol assimilation

To visualize the integration of methanol into the central metabolic pathways of the cells, the intracellular metabolic profile of the strain AM1 was analyzed. Therefore, a C¹³-methanol labeling experiment was conducted on the strain AM1 in MOPS medium supplemented with 50 mM xylose, 2% (wt/v) casein hydrolysate and 120 mM C¹³-methanol. The analysis identified key metabolites involved in carbon metabolism, including intermediates from the Embden-Meyerhof-Parnas (EMP) pathway, the tricarboxylic acid (TCA) cycle, and the pentose phosphate pathway (PPP)[35] (Fig 5A). After six days of cultivation, these metabolites displayed extensive labeling, with the majority incorporating three labeled carbon atoms, while a subset showed complete labeling across all carbon positions, indicating comprehensive metabolic integration. C¹³ labeling was observed in metabolites from the EMP pathway, with varying degrees of incorporation. Among these metabolites, labeling was detected in 80.7% of glucose 6-phosphate (G6P), 63.5% of fructose 6-phosphate (F6P), and 70.1% of fructose 1,6-bisphosphate (F1,6-P). Furthermore, 36.7% of 2-phosphoglyceric acid (2-PG), 35.7% of 3-phosphoglyceric acid (3-PG), 38.9% of phosphoenolpyruvic acid (PEP), and 48.3% of pyruvic acid (PYR) were labeled. In the TCA cycle, a substantial fraction of metabolites exhibited C¹³ labeling. Specifically, 64.1% of citric acid, 41.8% of cis-aconitic acid, 53.4% of succinic acid, 49.3% of fumaric acid, and 54.2% of malic acid were labeled. Additionally, the PPP pathway intermediates showed notable C¹³ labeling, with 41.4% of ribulose-5-phosphate (Ru5P) and 47.5% of sedoheptulose-7-phosphate (S7P) being labeled (Fig 5B). The methanol labeling experiment revealed that over 50% of the carbon atoms in central metabolites were labeled, providing evidence of the strain's efficient methanol assimilation ability.

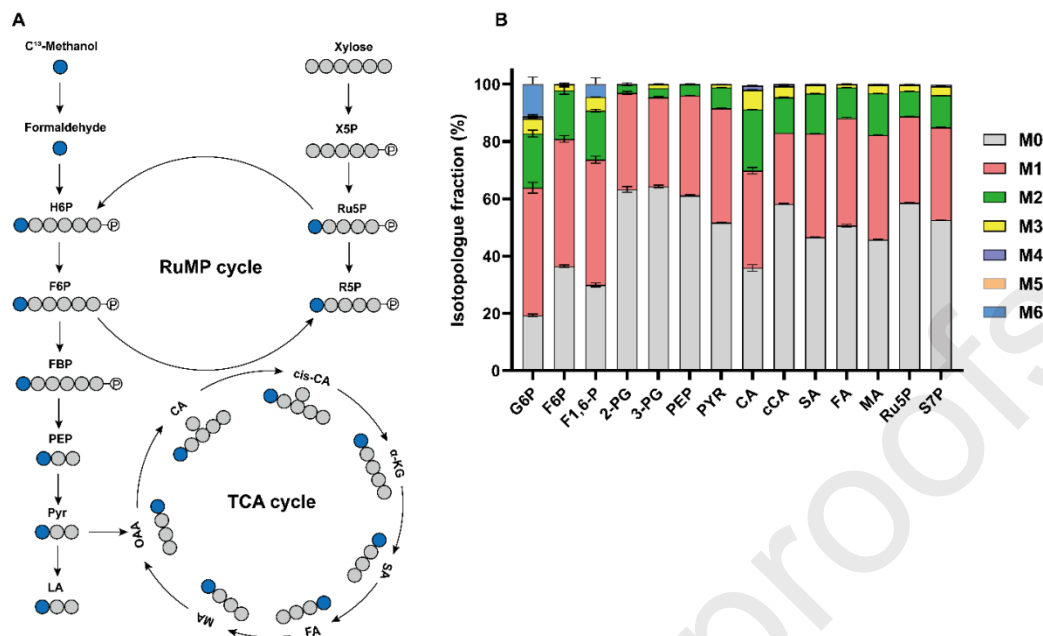


Fig. 5. Metabolic profile and Mechanisms in Efficient Methanol Assimilation. (A) A schematic diagram of metabolic pathways labeled with C-¹³ methanol, including the TCA cycle and PPP cycle. (B) Quantitative analysis of intracellular endogenous C-¹³-labeled methanol metabolites.

3.5 Efficient methanol assimilation for high-value product synthesis

To advance the practical application of efficient methanol-assimilating strain, its potential was explored in the biosynthesis of various high-value-added compounds. Among these compounds, 3-hydroxypropionate (3-HP) holds particular significance as a vital precursor for the synthesis of diverse chemicals, including acrylate and acrylamide, and as an essential monomer to produce biodegradable plastics[42]. Consequently, 3-HP has been designated by the United States Department of Energy (DOE) as one of the top 12 priority biobased building blocks, highlighting its industrial and scientific significance[43].

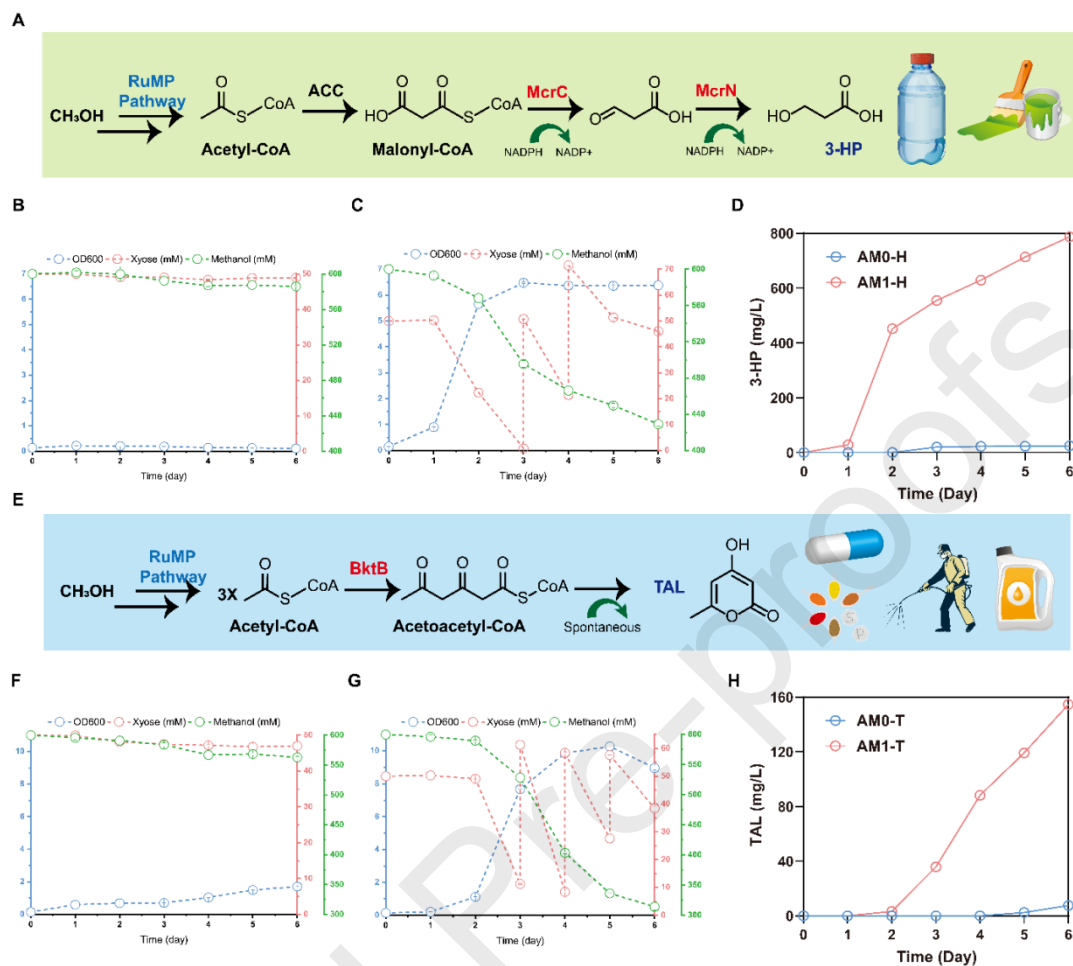


Fig. 6. Efficient methanol assimilation for high-value product synthesis. (A) Schematic diagram of the 3-hydroxypropionic acid (3-HP) synthesis pathway, and exhibition of derived industrial chemical products. (B) Growth, xylose and methanol consumption of the AM0-H during 3-HP fermentation. (C) Growth, xylose and methanol consumption of the AM1-H during 3-HP fermentation. (D) Analysis of 3-HP fermentation under the 600 mM methanol conditions. (E) Schematic diagram of the triacetic acid lactone (TAL) synthesis pathway and exhibition of derived industrial chemical products. (F) Growth, xylose and methanol consumption of the AM0-T during TAL fermentation. (G) Growth, xylose and methanol consumption of the AM1-T during TAL fermentation. (H) Analysis of TAL fermentation under the 600 mM methanol conditions.

Since *E. coli* cannot synthesize 3-HP on its own, a heterologous 3-HP synthesis pathway was introduced. The *mcrN* and *mcrC* genes encoding malonyl-CoA reductase from *Chloroflexus aurantiacus*[44] were cloned into plasmid pETduet-1 and transformed into AM1, yielding the engineered strain AM1-H. The AM0 strain harboring the *mcrC* and *mcrN* genes, designated as AM0-H, was used as the control strain. (Fig 6A). The strains were cultivated in MOPS medium containing 600 mM methanol, supplemented with 50 mM xylose and 2% (wt/v) casein hydrolysate. During 6 days of continuous cultivation, the strain AM0-H showed almost no growth, with the optical density (OD₆₀₀) remaining at the initial level of 0.1, and only consumed 1 mM xylose and 4 mM methanol (after accounting for the volatile portion of 11 mM) (Fig 6B). In contrast, the

strain AM1-H, despite the metabolic burden and toxic effects associated with the production of 3-HP[45], maintained an OD₆₀₀ of 6.4, consuming 104 mM xylose and 175 mM methanol (Fig 6C). Crucially, the strain AM0-H produced only 25 mg/L of 3-HP, as determined through analysis, the engineered strain AM1-H achieved a 3-HP production of 787 mg/L, which represents a 30.5-fold increase compared to the control strain AM0-H (Fig 6D).

Triacetic acid lactone (TAL) is widely regarded as a highly versatile platform chemical, offering considerable potential for the synthesis of a diverse array of molecular compounds. Its unique chemical properties and broad applicability make it a promising precursor for developing value-added products across various industrial and scientific domains[46]. The plasmid pTrc99a-*bktB*, harboring the *bktB* gene encoding thiolase (which catalyzes the conversion of acetyl-CoA to acetoacetyl-CoA, followed by spontaneous cyclization to form TAL[47]) (Fig 6E), was introduced into the AM0 and AM1 strains, resulting in strains AM0-T and AM1-T. The strains were cultured in MOPS medium supplemented with 600 mM methanol, 50 mM xylose, and 2% (wt/v) casein hydrolysate. The strain AM0-T exhibited limited growth and weak consumption of methanol and xylose, achieving an OD₆₀₀ of 1.7, with 3 mM xylose and 26 mM methanol consumed (Fig 6F). In contrast, the strain AM1-T demonstrated robust growth during TAL production, attaining an OD₆₀₀ of 9.0 and significantly depleting both xylose (142 mM) and methanol (303 mM) (Fig 6G). Notably, during the 6-day fermentation, the control strain AM0 produced only 8 mg/L of TAL, whereas the engineered strain AM1-T produced 155 mg/L, yielding a 19.3-fold increase relative to the control (Fig 6H).

4. Conclusion

Methanol is increasingly recognized as a pivotal substrate for the biomanufacturing industry, offering significant potential as a next-generation feedstock [48]. However, its effective utilization is often hindered by the cytotoxic effects of formaldehyde, a key intermediate in its assimilation. While natural microbes have evolved pathways to detoxify formaldehyde by converting it into formate and eventually CO₂ [6], these pathways are not directly applicable during methanol assimilation, primarily due to the loss of the formaldehyde intermediate [49]. Adaptive laboratory evolution (ALE) presents a potential solution by accumulating beneficial mutations, yet it often requires extensive timeframes and continuous oversight [50]. Moreover, these mutations may inadvertently reactivate formaldehyde dissimilation pathways, leading to further carbon losses [6].

Our study elucidates a novel formaldehyde toxicity mechanism wherein cellular exposure to formaldehyde triggers intracellular ROS accumulation, leading to DNA damage, protein degradation, and lipid peroxidation, ultimately culminating in cell death [17]. Notably, formaldehyde-induced cytotoxicity was markedly attenuated through the implementation of an exogenous ROS scavenging system. By integrating a modular ROS-scavenging system into the methanol-assimilating chassis strain, we established a robust platform demonstrating substantially enhanced methanol assimilation capacity. Furthermore, through a fed-batch strategy combining methanol and xylose supplementation, the engineered strain achieved a remarkable enhanced methanol assimilation level. Collectively, our findings underscore the scientific and biotechnological significance of ROS clearance systems in optimizing methanol assimilation, providing valuable insights for metabolic engineering and industrial biotechnology applications.

CRedit authorship contribution statement

Haiyan Liu: Writing – review & editing, Writing – original draft, Formal analysis, Data curation, Conceptualization. **Yun Chen:** Writing – review & editing, Data curation, Conceptualization. **Jian Li:** Writing – review & editing, Data curation. **Cheng Zhu:** Writing – review & editing, Resources, Methodology. **Jiahui Peng:** Writing – review & editing, Supervision. **Ramon Gonzalez:** Writing – review & editing, Supervision, Formal analysis. **Yanfen Bai:** Writing – review & editing, Supervision, Project administration, Formal analysis. **Zaigao Tan:** Writing – review & editing, Supervision, Project administration, Formal analysis, Funding acquisition

Declaration of competing interest

The authors declare that they have no known competing financial interests or personal relationships that could have appeared to influence the work reported in this paper.

Acknowledgments

This work has been financially supported by the National Natural Science Foundation of China (Project No. 32422047, 32371482, 32101175), Science and Technology Commission of Shanghai Municipality (Project No. 24HC2810800). The funders had no role in study design, data collection and analysis, decision to publish, or preparation of the manuscript.

Appendix A. Supplementary data

Figs. S1 to S8

Table S1 to S2

References

- [1] H. Zhang, X. Li, F. Zhu, K. Cen, C. Du, X. Tu, Plasma assisted dry reforming of methanol for clean syngas production and high-efficiency CO₂ conversion, *Chemical Engineering Journal* 310 (2017) 114-119. <https://doi.org/10.1016/j.cej.2016.10.104>.
- [2] T.J. Deka, A.I. Osman, D.C. Baruah, D.W. Rooney, Methanol fuel production, utilization, and techno-economy: a review, *Environmental Chemistry Letters* (2022).
- [3] J.Q. Gao, Y.X. Li, W. Yu, Y.J.J. Zhou, Rescuing yeast from cell death enables overproduction of fatty acids from sole methanol, *Nature Metabolism* 4(7) (2022) 932-943. <https://doi.org/10.1038/s42255-022-00601-0>.
- [4] L.C. Wirner, F. Kosaka, T. Sasayama, Y. Liu, A. Urakawa, K. Kuramoto, Combined capture and reduction of CO₂ to methanol using a dual-bed packed reactor, *Chemical Engineering Journal* 470 (2023). <https://doi.org/10.1016/j.cej.2023.144227>.
- [5] F.Y.H. Chen, H.W. Jung, C.Y. Tsuei, J.C. Liao, Converting *Escherichia coli* to a synthetic methylotroph growing solely on methanol, *Cell* 182(4) (2020) 933-946. <https://doi.org/10.1016/j.cell.2020.07.010>.
- [6] V.J. Klein, M. Irla, M.G. López, T. Brautaset, L.F. Brito, Unravelling formaldehyde metabolism in bacteria: road towards synthetic methylotrophy, *microorganisms* 10(2) (2022). <https://doi.org/ARTN22010.3390/microorganisms10020220>.
- [7] X. Wang, X.L. Wang, X.L. Lu, C. Ma, K.Q. Chen, P.K. Ouyang, Methanol fermentation increases the production of NAD(P)H-dependent chemicals in synthetic methylotrophic, *Biotechnol Biofuels* 12 (2019). <https://doi.org/ARTN1710.1186/s13068-019-1356-4>.
- [8] T. Gassler, M. Sauer, B. Gasser, M. Egermeier, C. Troyer, T. Causon, S. Hann, D. Mattanovich, M.G. Steiger, The industrial yeast *Pichia pastoris* is converted from a heterotroph into an autotroph capable of growth on CO₂, *Nature Biotechnology* 38(2) (2020) 210-216. <https://doi.org/10.1038/s41587-019-0363-0>.
- [9] H. He, R. Höper, M. Dodenhöft, P. Marlière, A. Bar-Even, An optimized methanol assimilation pathway relying on promiscuous formaldehyde-condensing aldolases in *E. coli*. *Metabolic Engineering* 60 (2020) 1-13. <https://doi.org/10.1016/j.ymben.2020.03.002>.
- [10] I.W. Bogorad, C.T. Chen, M.K. Theisen, T.Y. Wu, A.R. Schlenz, A.T. Lam, J.C. Liao, Building carbon-carbon bonds using a biocatalytic methanol condensation cycle, *P Natl Acad Sci USA* 111(45) (2014) 15928-15933. <https://doi.org/10.1073/pnas.1413470111>.
- [11] J.B. Siegel, A.L. Smith, S. Poust, A.J. Wargacki, A. Bar-Even, C. Louw, B.W. Shen, C.B. Eiben, H.M. Tran, E. Noor, J.L. Gallaher, J. Bale, Y. Yoshikuni, M.H. Gelb, J.D. Keasling, B.L. Stoddard, M.E. Lidstrom, D. Baker, Computational protein design enables a novel one-carbon assimilation pathway, *Proc Natl Acad Sci U S A* 112(12) (2015) 3704-9. <https://doi.org/10.1073/pnas.1500545112>.

- [12] X. Lu, Y. Liu, Y. Yang, S. Wang, Q. Wang, X. Wang, Z. Yan, J. Cheng, C. Liu, X. Yang, H. Luo, S. Yang, J. Gou, L. Ye, L. Lu, Z. Zhang, Y. Guo, Y. Nie, J. Lin, S. Li, C. Tian, T. Cai, B. Zhuo, H. Ma, W. Wang, Y. Ma, Y. Liu, Y. Li, H. Jiang, Constructing a synthetic pathway for acetyl-coenzyme A from one-carbon through enzyme design, *Nature Communications* 10(1) (2019) 1378. <https://doi.org/10.1038/s41467-019-09095-z>.
- [13] A. Chou, J.M. Clomburg, S. Qian, R. Gonzalez, 2-Hydroxyacyl-CoA lyase catalyzes acyloin condensation for one-carbon bioconversion, *Nature Chemical Biology* 15(9) (2019) 900-+. <https://doi.org/10.1038/s41589-019-0328-0>.
- [14] T. Cai, H. Sun, J. Qiao, L. Zhu, F. Zhang, J. Zhang, Z. Tang, X. Wei, J. Yang, Q. Yuan, W. Wang, X. Yang, H. Chu, Q. Wang, C. You, H. Ma, Y. Sun, Y. Li, C. Li, H. Jiang, Q. Wang, Y. Ma, Cell-free chemoenzymatic starch synthesis from carbon dioxide, *Science* 373(6562) (2021) 1523-1527. <https://doi.org/10.1126/science.abh4049>.
- [15] A. Chou, S.H. Lee, F. Zhu, J.M. Clomburg, R. Gonzalez, An orthogonal metabolic framework for one-carbon utilization, *Nat Metab* 3(10) (2021) 1385-1399. <https://doi.org/10.1038/s42255-021-00453-0>.
- [16] M.K. Li, W.J. Sun, X. Wang, K.Q. Chen, Y. Feng, Z.G. Tan, A eukaryote-featured membrane phospholipid enhances bacterial formaldehyde tolerance and assimilation of one-carbon feedstocks, *Acs Synthetic Biology* (2024). <https://doi.org/10.1021/acssynbio.4c00499>.
- [17] L.A. Johnson, L.A. Hug, Distribution of reactive oxygen species defense mechanisms across domain bacteria, *Free Radic Biol Med* 140 (2019) 93-102. <https://doi.org/10.1016/j.freeradbiomed.2019.03.032>.
- [18] Y. Jiang, B. Chen, C. Duan, B. Sun, J. Yang, S. Yang, Multigene editing in the *Escherichia coli* genome via the CRISPR-Cas9 system, *Appl Environ Microbiol* 81(7) (2015) 2506-14. <https://doi.org/10.1128/AEM.04023-14>.
- [19] K.A. Datsenko, B.L. Wanner, One-step inactivation of chromosomal genes in *Escherichia coli* K-12 using PCR products, *Proc Natl Acad Sci U S A* 97(12) (2000) 6640-5. <https://doi.org/10.1073/pnas.120163297>.
- [20] N.S. Kolber, R. Fattal, S. Bratulic, G.D. Carver, A.H. Badran, Orthogonal translation enables heterologous ribosome engineering in *E. coli*, *Nat Commun* 12(1) (2021) 599. <https://doi.org/10.1038/s41467-020-20759-z>.
- [21] Z. Tan, J. Chen, X. Zhang, Systematic engineering of pentose phosphate pathway improves *Escherichia coli* succinate production, *Biotechnol Biofuels* 9 (2016) 262. <https://doi.org/10.1186/s13068-016-0675-y>.
- [22] F.C. Neidhardt, P.L. Bloch, D.F. Smith, Culture Medium for Enterobacteria, *Journal of Bacteriology* 119(3) (1974) 736-747. <https://doi.org/doi:10.1128/jb.119.3.736-747.1974>.
- [23] N.-X. Lin, R.-Z. He, Y. Xu, X.-W. Yu, Oxidative stress tolerance contributes to heterologous protein production in *Pichia pastoris*, *Biotechnology for Biofuels* 14(1) (2021). <https://doi.org/10.1186/s13068-021-02013-w>.
- [24] C. Zhan, X. Li, G. Lan, E.E.K. Baidoo, Y. Yang, Y. Liu, Y. Sun, S. Wang, Y. Wang, G. Wang, J. Nielsen, J.D. Keasling, Y. Chen, Z. Bai, Reprogramming methanol utilization pathways to convert *Saccharomyces cerevisiae* to a synthetic methylotroph, *Nature Catalysis* 6(5) (2023) 435-450. <https://doi.org/10.1038/s41929-023-00957-w>.

- [25] S. Kim, S.N. Lindner, S. Aslan, O. Yishai, S. Wenk, K. Schann, A. Bar-Even, Growth of *E. coli* on formate and methanol via the reductive glycine pathway, *Nat Chem Biol* 16(5) (2020) 538-545. <https://doi.org/10.1038/s41589-020-0473-5>.
- [26] P. Giavalisco, Y. Li, A. Matthes, A. Eckhardt, H.M. Hubberten, H. Hesse, S. Segu, J. Hummel, K. Kohl, L. Willmitzer, Elemental formula annotation of polar and lipophilic metabolites using (13) C, (15) N and (34) S isotope labelling, in combination with high-resolution mass spectrometry, *Plant J* 68(2) (2011) 364-76. <https://doi.org/10.1111/j.1365-313X.2011.04682.x>.
- [27] N. Qin, L. Li, X. Wan, X. Ji, Y. Chen, C. Li, P. Liu, Y. Zhang, W. Yang, J. Jiang, J. Xia, S. Shi, T. Tan, J. Nielsen, Y. Chen, Z. Liu, Increased CO₂ fixation enables high carbon-yield production of 3-hydroxypropionic acid in yeast, *Nat Commun* 15(1) (2024) 1591. <https://doi.org/10.1038/s41467-024-45557-9>.
- [28] J. Yu, J. Landberg, F. Shavarebi, V. Bilanchone, A. Okerlund, U. Wanninayake, L. Zhao, G. Kraus, S. Sandmeyer, Bioengineering triacetic acid lactone production in *Yarrowia lipolytica* for pogostone synthesis, *Biotechnol Bioeng* 115(9) (2018) 2383-2388. <https://doi.org/10.1002/bit.26733>.
- [29] J.M. McCord, I. Fridovich, Superoxide Dismutase, *Journal of Biological Chemistry* 244(22) (1969) 6049-6055. [https://doi.org/10.1016/s0021-9258\(18\)63504-5](https://doi.org/10.1016/s0021-9258(18)63504-5).
- [30] V.B. Borisov, S.A. Siletsky, M.R. Nastasi, E. Forte, ROS defense systems and terminal oxidases in bacteria, *Antioxidants (Basel)* 10(6) (2021). <https://doi.org/10.3390/antiox10060839>.
- [31] T.E. Saleski, M.T. Chung, D.N. Carruthers, A. Khasbaatar, K. Kurabayashi, X.N. Lin, Optimized gene expression from bacterial chromosome by high-throughput integration and screening, *Science Advances* 7(7) (2021) eabe1767. <https://doi.org/doi:10.1126/sciadv.abe1767>.
- [32] Y. Wang, R. Branicky, A. Noe, S. Hekimi, Superoxide dismutases: Dual roles in controlling ROS damage and regulating ROS signaling, *J Cell Biol* 217(6) (2018) 1915-1928. <https://doi.org/10.1083/jcb.201708007>.
- [33] F. Yuan, S. Yin, Y. Xu, L. Xiang, H. Wang, Z. Li, K. Fan, G. Pan, The richness and diversity of catalases in bacteria, *Front Microbiol* 12 (2021) 645477. <https://doi.org/10.3389/fmicb.2021.645477>.
- [34] T.Y. Wu, C.T. Chen, J.T. Liu, I.W. Bogorad, R. Damoiseaux, J.C. Liao, Characterization and evolution of an activator-independent methanol dehydrogenase from *Cupriavidus necator* N-1, *Appl Microbiol Biotechnol* 100(11) (2016) 4969-83. <https://doi.org/10.1007/s00253-016-7320-3>.
- [35] X. Wang, X. Wang, X. Lu, C. Ma, K. Chen, P. Ouyang, Methanol fermentation increases the production of NAD(P)H-dependent chemicals in synthetic methylotrophic *Escherichia coli*, *Biotechnol Biofuels* 12 (2019) 17. <https://doi.org/10.1186/s13068-019-1356-4>.
- [36] F.Y. Chen, H.W. Jung, C.Y. Tsuei, J.C. Liao, Converting *Escherichia coli* to a synthetic methylotroph growing solely on methanol, *Cell* 182(4) (2020) 933-946 e14. <https://doi.org/10.1016/j.cell.2020.07.010>.

- [37] C.T. Chen, F.Y. Chen, I.W. Bogorad, T.Y. Wu, R. Zhang, A.S. Lee, J.C. Liao, Synthetic methanol auxotrophy of *Escherichia coli* for methanol-dependent growth and production, *Metab Eng* 49 (2018) 257-266. <https://doi.org/10.1016/j.ymben.2018.08.010>.
- [38] W. Zhang, T. Zhang, M. Song, Z. Dai, S. Zhang, F. Xin, W. Dong, J. Ma, M. Jiang, Metabolic engineering of *Escherichia coli* for high yield production of succinic acid driven by methanol, *ACS Synth Biol* 7(12) (2018) 2803-2811. <https://doi.org/10.1021/acssynbio.8b00109>.
- [39] R.K. Bennett, M. Dillon, J.R. Gerald Har, A. Agee, B. von Hagel, J. Rohllhill, M.R. Antoniewicz, E.T. Papoutsakis, Engineering *Escherichia coli* for methanol-dependent growth on glucose for metabolite production, *Metab Eng* 60 (2020) 45-55. <https://doi.org/10.1016/j.ymben.2020.03.003>.
- [40] W.B. Whitaker, J.A. Jones, R.K. Bennett, J.E. Gonzalez, V.R. Vernacchio, S.M. Collins, M.A. Palmer, S. Schmidt, M.R. Antoniewicz, M.A. Koffas, E.T. Papoutsakis, Engineering the biological conversion of methanol to specialty chemicals in *Escherichia coli*, *Metab Eng* 39 (2017) 49-59. <https://doi.org/10.1016/j.ymben.2016.10.015>.
- [41] R.K. Bennett, J.E. Gonzalez, W.B. Whitaker, M.R. Antoniewicz, E.T. Papoutsakis, Expression of heterologous non-oxidative pentose phosphate pathway from *Bacillus methanolicus* and phosphoglucose isomerase deletion improves methanol assimilation and metabolite production by a synthetic *Escherichia coli* methylotroph, *Metab Eng* 45 (2018) 75-85. <https://doi.org/10.1016/j.ymben.2017.11.016>.
- [42] W. Yu, X. Cao, J. Gao, Y.J. Zhou, Overproduction of 3-hydroxypropionate in a super yeast chassis, *Bioresour Technol* 361 (2022) 127690. <https://doi.org/10.1016/j.biortech.2022.127690>.
- [43] S. Choi, C.W. Song, J.H. Shin, S.Y. Lee, Biorefineries for the production of top building block chemicals and their derivatives, *Metab Eng* 28 (2015) 223-239. <https://doi.org/10.1016/j.ymben.2014.12.007>.
- [44] C. Liu, Q. Wang, M. Xian, Y. Ding, G. Zhao, Dissection of malonyl-coenzyme A reductase of *Chloroflexus aurantiacus* results in enzyme activity improvement, *PLoS One* 8(9) (2013) e75554. <https://doi.org/10.1371/journal.pone.0075554>.
- [45] J. Mao, H. Zhang, Y. Chen, L. Wei, J. Liu, J. Nielsen, Y. Chen, N. Xu, Relieving metabolic burden to improve robustness and bioproduction by industrial microorganisms, *Biotechnol Adv* 74 (2024) 108401. <https://doi.org/10.1016/j.biotechadv.2024.108401>.
- [46] Z. Tan, J.M. Clomburg, S. Cheong, S. Qian, R. Gonzalez, A polyketoacyl-CoA thiolase-dependent pathway for the synthesis of polyketide backbones, *Nature Catalysis* 3(7) (2020) 593-603. <https://doi.org/10.1038/s41929-020-0471-8>.
- [47] Z. Tan, X. Zhu, J. Chen, Q. Li, X. Zhang, Activating phosphoenolpyruvate carboxylase and phosphoenolpyruvate carboxykinase in combination for improvement of succinate production, *Appl Environ Microbiol* 79(16) (2013) 4838-44. <https://doi.org/10.1128/AEM.00826-13>.
- [48] W. Jiang, D. Hernandez Villamor, H. Peng, J. Chen, L. Liu, V. Haritos, R. Ledesma-Amaro, Metabolic

engineering strategies to enable microbial utilization of C1 feedstocks, *Nat Chem Biol* 17(8) (2021) 845-855. <https://doi.org/10.1038/s41589-021-00836-0>.

[49] A. Sarwar, E.Y. Lee, Methanol-based biomanufacturing of fuels and chemicals using native and synthetic methylotrophs, *Synth Syst Biotechnol* 8(3) (2023) 396-415. <https://doi.org/10.1016/j.synbio.2023.06.001>.

[50] Q. Sun, D.h. Liu, Z. Chen, Engineering and adaptive laboratory evolution of *Escherichia coli* for improving methanol utilization based on a hybrid methanol assimilation pathway, *Frontiers in Bioengineering and Biotechnology* 10 (2023).

Highlights

Uncovered a novel mechanism of formaldehyde toxicity

Reactive oxygen species detoxification boosts formaldehyde tolerance in cells

Reactive oxygen species scavenging system integrates superoxide dismutase and catalase

Reactive oxygen species scavenging system enhances methanol assimilation efficiency